Progress In Electromagnetics Research C, Vol. 82, 77–88, 2018

Structural and Magnetic Studies of $Fe_{100-x}Co_x$ Nanotubes Obtaine by Template Method

Kayrat K. Kadyrzhanov[1, 2], Vyacheslav S. Rusakov[3], Artem L. Kozlovskiy[1, 2, *], Maxim V. Zdorovets[1, 2, 4], Egor Y. Kaniukov[5], Alena E. Shumskaya[5], Inesh E. Kenzhina[1, 2], and Maxim S. Fadeev[3]

Abstract—Hollow nanostructures based on the $Fe_{100-x}Co_x$ alloy were synthesized in the pores of polymer template matrices based on PET using the electrochemical deposition method. Morphology, elemental composition, and structural features were characterized by scanning electron microscopy, energy dispersive analysis, and X-ray diffractometry. The study of the internal magnetic texture was carried out using Mossbauer spectroscopy. The dependence of the change in structural and magnetic properties from the atomic content of components in nanotube structure is revealed. It is established that the synthesized nanostructures are hollow $Fe_{100-x}Co_x$ nanotubes with a body-centered cubic crystal structure. The decrease in the unit cell parameter with increasing cobalt concentration is due to the difference in the radii of Fe (1.227 Å) and Co (1.191 Å) atoms. It is established that a random distribution of magnetic moments directions of Fe atoms is observed for $Fe_{100}Co_0$ nanotubes. And magnetic texture along the nanotube axis is observed for $Fe_{100-x}Co_x$ nanotubes, with an increase in Co atoms concentration. The average angle between the direction of the magnetic moment of iron atoms and the nanotube axis decreases from $\vartheta = 54.6°$ to $\vartheta = 24.5°$.

1. INTRODUCTION

Recently, obtaining nanostructured materials is one of the most attractive research directions, mainly because of the wide field of potential applications of nanostructures, from microelectronics, information storage and communication to biotechnology [1–5]. Nanostructures are actual, not only because they allow miniaturization of devices, but also because materials constructed at the nanoscale show properties that are very different from macro-sized objects [6–9]. One of the important problems of modern materials science is the production of nanomaterials, which includes both scientific and technological aspects. The way of production influences the structural and magnetic properties of synthesized nanomaterials [10–12]. The magnetic properties of nanostructures are different from the properties of bulk materials, while reducing the average size of nanostructures comparable to the width of the magnetic domain is of greatest interest for potential practical applications. Also, important factors in changing the magnetic texture of nanomaterials are factors such as geometric characteristics and crystal structure [13, 14]. The choice of materials based on iron-cobalt was made because of the potential use of nanostructures in various applications, for example, in catalysis [15], biomedicine [16], magnetic carriers of media [17].

Received 5 December 2017, Accepted 3 March 2018, Scheduled 13 March 2018

* Corresponding author: Artem Leonidovich Kozlovskiy (artem88sddt@mail.ru).

[1] L.N. Gumilyov Eurasian National University, Satpayev Str., 2, Astana 010008, Republic of Kazakhstan. [2] Institute of Nuclear Physics, 1, Ibragimov St., Almaty 050032, Republic of Kazakhstan. [3] M.V. Lomonosov Moscow State University, Leninskie Gory, 1, bld. 2, Moscow 119991, Russian Federation. [4] Ural Federal University, 19 Mira St., Yekaterinburg 620002, Russian Federation. [5] SSPA "Scientific-Practical Materials Research Centre of NAS of Belarus", 19 P. Brovki Str., Minsk 220072, Republic of Belarus.

The paper presents the results of a systematic study of structural and magnetic properties of $Fe_{100-x}Co_x$ nanotubes obtained by electrochemical synthesis. Morphology, element composition and structural features were characterized by scanning electron microscopy, energy dispersive analysis, and X-ray diffractometry. The study of the internal magnetic texture was carried out using Mossbauer spectroscopy.

2. EXPERIMENTAL PART

The track membranes used as the template matrix were made of PET film of Hostaphan® brand manufactured by Mitsubishi Polyester Film (Germany). The films were irradiated at heavy ion DC-60 accelerator (Astana, Kazakhstan) with krypton ions with an energy of 1.75 MeV/nucleon and a fluence of $1 \cdot 10^9$ ion/cm^2 [18]. After irradiation, the polymer films were chemically etched for 70 s in a 2.2 M NaOH solution. These conditions and the etching time made it possible to obtain track membranes with cylindrical pores with a diameter of $\sim 110 \pm 5$ nm, which do not form conglomerates of crossed or merged pores [19]. The choice of the method of electrochemical deposition is due to the simplicity of scaling and the ability to control the physical-chemical properties of synthesized nanostructures.

2.1. Electrochemical Synthesis of Nanostructures

The electrochemical deposition in PET nanopores was carried out in potentiostatic mode at a voltage of 2.0 V. The composition of the electrolyte solution for the preparation of iron and iron-cobalt nanostructures is the following: 7-aqueous ferrous and cobalt sulfates — $FeSO_4 \times 7H_2O$, $CoSO_4 \times 7H_2O$ in the required molar ratio, and 6-water ferric chloride — $FeCl_2 \times 6H_2O$, boric chloride-H_3BO_3 and ascorbic acid $C_6H_8O_6$. All used chemical reagents had a purity of analytical or reagent grade. The growth of nanostructures was monitored by the chronoamperometry method using the Agilent 34410A multimeter. Since the template matrix is a dielectric, a layer of 10 nm gold was deposited to create a conductive layer on the matrix by magnetron sputtering in a vacuum, which served as a working electrode (cathode) during deposition. Under these conditions of sputtering, the pores in matrix remain open, which made it possible to obtain nanosystems in the form of nanotubes. For PET-based templates, the maximum possible porosity is 15% at a pore density of 10^9 pores/cm^2 and a diameter of 110 nm. The equivalent area of the electrode surface was 6.0×10^{-6} m^2, with a total membrane area of 4.0×10^{-4} m^2. Templates with the same area were used for all experiments.

2.2. Investigation of Morphology and Structural Properties

The structural characteristics and elemental composition of the nanotubes were studied using a Hitachi TM3030 scanning electron microscope with a Bruker XFlash MIN SVE microanalysis system at an accelerating voltage of 15 kV. X-ray diffraction analysis (XRD) was performed on a D8 ADVANCE ECO diffractometer (Bruker, Germany) using CuKα radiation. The software BrukerAXSDIFFRAC.EVAv.4.2 and the international ICDD PDF-2 database were used to identify the phases and study the crystal structure.

2.3. Measurement of Magnetic Characteristics

A universal measuring system (automated vibration magnetometer) "Liquid Helium Free High Field Measurement System" ("Cryogenic LTD", London, UK) was used to measure the magnetic characteristics of the substance. The measurements were performed by an induction method, by measuring the induced electromotive force of induction in the signal coils with a magnetized sample oscillating with a certain frequency, when the temperature and external magnetic field were recorded at in-situ with measurement. This method provides an error in the result of measuring the magnetization not worse than 1.5% for a measurable magnetization value of not less than $\pm 1 \cdot 10^{-6}$ A·m^2 ($\pm 1 \cdot 10^{-3}$ A·m^2).

The Mossbauer studies were carried out using a spectrometer MS1104Em operating in the mode of constant accelerations with a triangular shape of the Doppler velocity of the source relative to the absorber. The ^{57}Co nuclei in the Rh matrix acted as a source. The Mossbauer spectrometer was

calibrated at room temperature with a standard α-Fe absorber. For the processing and analysis of Mossbauer spectra, methods were used for reconstructing the distributions of the hyperfine parameters of the Mossbauer spectrum and model interpretation of the spectrum, taking into account the a priori information about the object of the study, realized in the SpectrRelax program [20].

3. RESULTS AND DISCUSSION

3.1. Morphology and Element Composition

Scanning electron microscopy (SEM) was used to study the morphology of synthesized nanotubes. Before the study, the samples were released from the polymer matrix, by dissolving the polymer in a solution of 9.0 M NaOH at a temperature of 60°C for 1 hour. The samples were washed in solutions of acetic acid and deionized water in an ultrasonic bath for 5 minutes to remove polymer residues after dissolution. The washing procedure was repeated three times. We used an electron beam with an electron energy of 2.0 keV in the LEI scanning mode to study the sample surface.

SEM micrographs confirm the homogeneous and regular structure of nanotubes. The geometric characteristics (diameter and length) of the nanotubes were measured using SEM. Analysis of SEM images obtained nanostructures showed that the height of nanotubes is equal to the thickness of the template of 12 µm, and the diameter of 110 nm. Analysis of the internal diameters of the nanotubes obtained was not carried out due to the insufficient SEM resolution.

The study of nanostructures internal diameters in PET templates was conducted by the manometric method for determining gas permeability. This method is based on measuring the molar density of the air flow Q as a function of the pressure difference Δp in the closed chamber on both sides of the template. That varied in the range from 0.008 to 0.020 MPa in steps of 0.004 MPa. The diameters d were determined in accordance with the Fick law from the relation (1) [21]:

$$Q = \frac{nd^3}{6l}\sqrt{\frac{2\pi}{\mathrm{RTM}}}\Delta p, \tag{1}$$

where Q is the gas volume passed through the nanotubes [m^3/h], r the pore radius [m], M the molar mass [kg/mol], R the universal gas constant [J/mol×K], T the temperature [K], n the pore density [$1/m^2$], l the membrane thickness [m], and Δp the applied air pressure [Pa]. The resulting average value of pore diameter of the PET template was 110 nm, which is in good agreement with the data obtained as a result of SEM studies of template matrices. Wall thicknesses of $Fe_{100-x}Co_x$ nanotubes are shown in Table 1. It is seen that wall thickness slightly increases with an increase of Co atoms in nanotubes.

Table 1. Geometric characteristics of $Fe_{100-x}Co_x$ nanotubes.

Nanotubes composition $Fe_{100-x}Co_x$	External diameter, nm	Internal diameter, nm	Wall thickness, nm
Fe_{100}	110	80	15
$Fe_{80}Co_{20}$		79	15
$Fe_{60}Co_{40}$		78	16
$Fe_{40}Co_{60}$		75	17
$Fe_{20}Co_{80}$		74	18

The EDS methods were used to determine the elemental composition. Table 2 shows the data of the elemental composition. The reliability of the results was confirmed by taking spectra from five points along the surface of investigated sample, as well as taking the distribution maps of the elements in structure using the mapping method.

As can be seen from the presented data, the atomic ratio of components in synthesized samples corresponds to the weight ratio of electrolyte components used for the synthesis. It can be seen that the elemental composition is retained along the entire length of the tube (Figure 1(b)). Thus, the

Table 2. Elemental analysis of synthesized samples.

Nanotubes composition $Fe_{100-x}Co_x$	Atomic weight of Fe, %	Error, %	Atomic weight of Co, %	Error, %
Fe_{100}	100	1,2	–	–
$Fe_{80}Co_{20}$	82,5	1,1	17,5	0,4
$Fe_{60}Co_{40}$	59,5	0,5	40,5	0,4
$Fe_{40}Co_{60}$	40,3	0,4	59,7	0,6
$Fe_{20}Co_{80}$	18,9	0,2	81,1	1,0

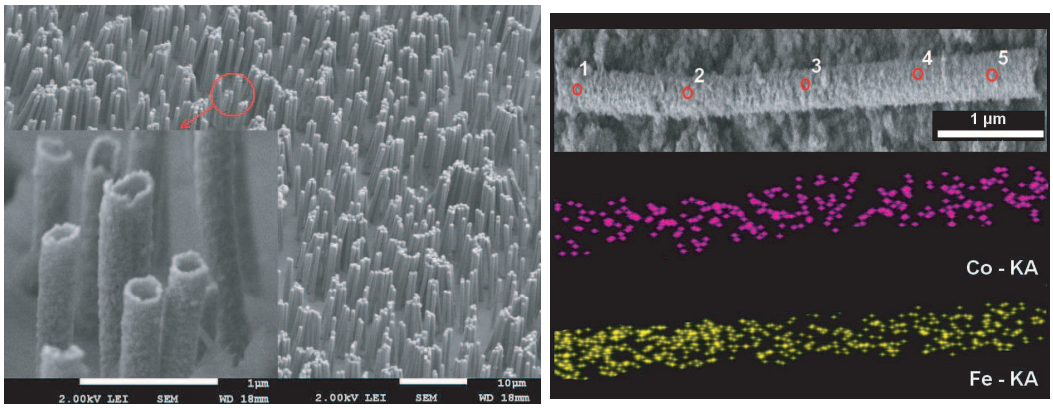

(a) (b)

Figure 1. (a) SEM results of $Fe_{100-x}Co_x$ nanotubes; (b) Example of element analysis results: 1 — $Fe_{59,45}Co_{40,55}$, 2 — $Fe_{59,37}Co_{40,63}$, 3 — $Fe_{58,95}Co_{41,05}$, 4 — $Fe_{59,58}Co_{40,42}$, 5 — $Fe_{58,79}Co_{41,21}$.

application of the electrochemical deposition method under given conditions makes it possible to obtain hollow nanostructures with given geometric properties and a controlled atomic ratio.

3.2. Crystal Structure

XRD was performed to clarify the parameters of the crystal structure. Figure 2 shows X-ray diffraction patterns of synthesized samples. The peaks shape indicates the polycrystalline structure of $Fe_{100-x}Co_x$ nanotubes. Most of the synthesized nanostructures are $Fe_{100-x}Co_x$ nanotubes with a body-centered cubic (bcc) crystal structure (spatial group). According to the published data, the bcc structure is typical for $Fe_{100-x}Co_x$ nanotubes with a Co content of less than 90% [22, 23] and films with a cobalt content of $< 85\%$ [24].

As a result of processing the obtained X-ray diffractograms, the unit cell parameters for investigated samples were determined. The crystal lattice parameter was calculated using the Nelson-Taylor extrapolation function (2) [25]:

$$a = f\left[\frac{1}{2}\left(\frac{\cos^2\theta}{\sin\theta} + \frac{\cos^2\theta}{\theta}\right)\right], \tag{2}$$

The value and error in determining the parameter a are defined by linear extrapolation of this function to the zero value of argument ($\theta = 90°$). The results of the change in main characteristics of the crystal structure for investigated samples are presented in Table 3.

As can be seen, with an increase in cobalt concentration in $Fe_{100-x}Co_x$ nanotubes structure, the crystal lattice parameter a decreases linearly with a coefficient $\partial a/\partial x = -0.32 \pm 0.02$ Å. The decrease in the unit cell parameter is due to the difference in radii of Fe (1.227 Å) and Co (1.191 Å) atoms.

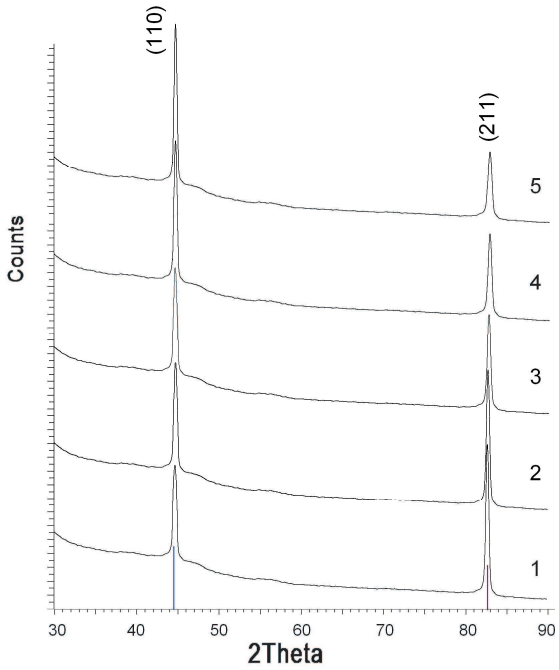

Figure 2. XRD diffractograms of the investigated samples of $Fe_{100-x}Co_x$ nanotubes: 1) $Fe_{100}Co_0$; 2) $Fe_{82.5}Co_{17.5}$; 3) $Fe_{59.5}Co_{40.5}$; 4) $Fe_{40.3}Co_{59.7}$; 5) $Fe_{18.9}Co_{81.1}$.

Table 3. Data of changes in characteristics of the crystal structure.

Nanotubes composition $Fe_{100-x}Co_x$	a, Å	TC_{hkl}	
		(110)	(211)
Fe_{100}	2.8627	**1.1262**	0.8737
$Fe_{80}Co_{20}$	2.8579	**1.2156**	0.8313
$Fe_{60}Co_{40}$	2.8501	**1.4933**	0.5066
$Fe_{40}Co_{60}$	2.8471	**1.4973**	0.4917
$Fe_{20}Co_{80}$	2.8421	**1.5017**	0.4841

The change in the intensity and shape of the diffraction peaks can be due to imperfection of the crystal structure, as well as to defects formed during the nanotubes synthesis.

During the synthesis of nanotubes with increasing cobalt concentration, a large number of defects are formed in the crystal structure, due to the difference between the diameters of the radii of iron and cobalt atoms. Also, an increase in the concentration of cobalt results in the appearance of a highlighted texture direction in the (110) direction. According to the X-ray data, a change in FWHM is observed for different planes with an increase in the atomic content of cobalt in the structure. The change in the FWHM of the main diffraction line (110) on X-ray patterns indicates an increase in the degree of crystallinity and the improvement of crystal structure with a decrease in the atomic iron content in nanotubes.

Determination of the dynamics of the change in texture planes and orientation of $Fe_{100-x}Co_x$ nanotubes as a result of irradiation was carried out by calculating the texture coefficients using the Harris Equation (3) [26]:

$$TC_{hkl} = \frac{I_{hkl}}{I_{0hkl}} \Big/ \frac{1}{n} \sum \frac{I_{hkl}}{I_{0hkl}}, \tag{3}$$

where I_{hkl} is the experimentally obtained intensity of the reflex, I_{0hkl} the corresponding intensity

according to the JCPDS database, and n the number of reflexes. Texture coefficients greater than one point to the predominant orientation of the array of nanotubes along the corresponding directions, which implies an increase in the number of grains along these directions (Table 3). The number of reflections (n) corresponds to the maximum value of texture coefficients. The TC_{hkl} values of investigated $Fe_{100-x}Co_x$ nanotubes confirm the assumption of the polycrystalline structure of nanotubes. With an increase in the Co concentration in the structure shows an increase in the texture coefficients for the (110) plane, which indicates the appearance of a distinguished direction in the crystal structure of $Fe_{100-x}Co_x$ nanotubes.

3.3. Magnetic Properties

Studies on crystal structure and magnetic characteristics have their value for the potential use of nanostructures as magnetic storage devices. In this case, the ability to control magnetic properties by changing the synthesis conditions opens up wide possibilities for scaling the process of obtaining magnetic nanostructures for the industry. Measurements of the dependence of magnetization from the applied magnetic field $M(H)$ for the parallel and perpendicular field directions with respect to the nanotube axis were carried out at room temperature (Figure 3). It has been established that $M(H)$ curves taken at various directions of the magnetic field have significant differences: in the parallel field, the loops are more shallow, their width is much larger. Based on the presented graphs of field dependences, the main magnetic characteristics (H_c — coercivity, M_r — residual magnetization, M_s — saturation magnetization, M_r/M_s — rectangularity coefficient of the hysteresis loop) were determined, which are given in Table 4.

Clear anisotropy of properties is observed for samples containing cobalt, which is explained by the anisotropy of the shape and is characteristic of nanomaterials with a large aspect ratio (~ 100). The axis of easy magnetization coincides with the axis of nanotubes. Regarding separately the values of the magnetic parameters for the two-component sample, it can be noted that there is no significant difference in the values. This can be explained by the presence of oxide amorphous phases of iron.

Table 4. The main magnetic characteristics of $Fe_{100-x}Co_x$ nanotubes for two directions of the magnetic field.

Nanotubes composition $Fe_{100-x}Co_x$	The magnetic field is parallel to the axis of $Fe_{100-x}Co_x$ nanotubes				The magnetic field is perpendicular to the axis of $Fe_{100-x}Co_x$ nanotubes			
	H_{Cll}	M_{rII}	M_{sII}	M_{rll}/M_{sll}	$H_{C\perp}$	$M_{r\perp}$	$M_{s\perp}$	$M_{r\perp}/M_{s\perp}$
Fe	100	6,6	137	0,23	310	31	135	0,05
$Fe_{80}Co_{20}$	410	33	103	0,32	150	7	109	0,06
$Fe_{60}Co_{40}$	600	28	56	0,5	70	14	51	0,27
$Fe_{40}Co_{60}$	590	55	110	0,5	64	2,2	100	0,02
$Fe_{20}Co_{80}$	250	10	136	0,41	100	75	132	0,03

Table 5. Results of calculations of effective anisotropy.

Nanotubes composition $Fe_{100-x}Co_x$	K_{eff}, 10^{-4} erg/cm^2
Fe	−2.59
$Fe_{80}Co_{20}$	−1.46
$Fe_{60}Co_{40}$	−0.43
$Fe_{40}Co_{60}$	−1.67
$Fe_{20}Co_{80}$	−2.55

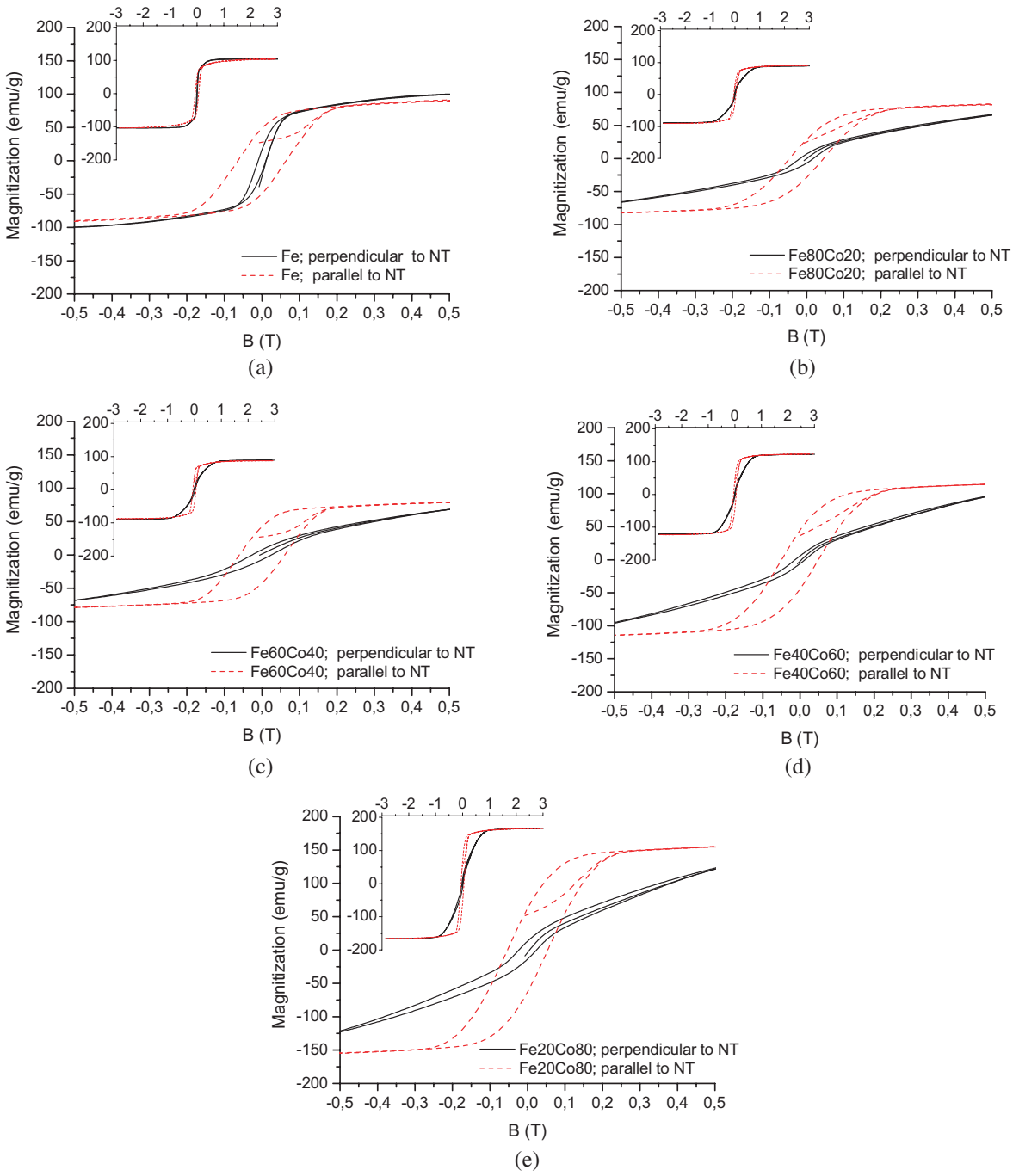

Figure 3. Magnetic properties. Hysteresis loops of Ni NTs arrays in PET template obtained in magnetic field parallel (black dotted line) and perpendicular oriented (red solid line) to the NTs axis at room temperatures: (a) $Fe_{100}Co_0$; (b) $Fe_{82.5}Co_{17.5}$; (c) $Fe_{59.5}Co_{40.5}$; (d) $Fe_{40.3}Co_{59.7}$; (e) $Fe_{18.9}Co_{81.1}$.

When analyzing the magnetic characteristics of $Fe_{100-x}Co_x$ nanotubes, the difference in magnetic parameters values of obtained samples is clearly visible. In magnetic nanostructures, there are many demagnetization mechanisms, and depending on the type of action, the magnetic moments change their direction with respect to the external field. The coefficient of effective magnetic anisotropy K_{eff} was calculated according to formula (4) [27]:

$$K_{eff} = \pi M_s^2(1-3P) + K_1, \tag{4}$$

where πM_s^2 is the shape demagnetization energy, K_1 the magnetically crystalline anisotropy energy, and $-3\pi M_s^2 P$ correspond to dipolar energy. Table 5 shows the results of K_{eff} calculations.

As can be seen from the presented data, with a change in Co concentration in structure, K_{eff} lies in the range from -2.59 to $-0.43\,\mathrm{erg/cm^2}$, according to the published data [27, 28] with $K_{eff} < 1$. The light axis of magnetization is displaced perpendicular to the nanotube axis, which indicates the anisotropy of magnetic domains. The coefficient of rectangularity of the hysteresis loop, like the coercivity, depends on the anisotropy of the nanotubes shape $Fe_{100-x}Co_x$ and in parallel fields is expected to exceed the values in perpendicular fields. Thus, a comparison of the magnetic characteristics for different orientations of magnetic field indicates that the values of $H_{c||}$ and $M_{r||}/M_{s||}$ higher than $H_{c\perp}$ and $M_{r\perp}/M_{s\perp}$ due to the anisotropy of the nanotube shape, which have an aspect ratio of ~ 100. It is worth noting that due to the presence of crystallographic anisotropy, the sample is easier to magnetize along the axis of $Fe_{100-x}Co_x$ nanotubes than perpendicular to it, which ensures predictability of the behavior of

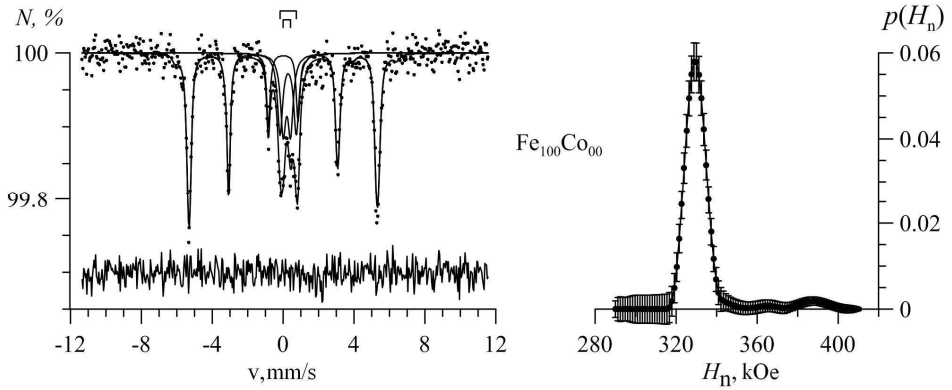

(a)

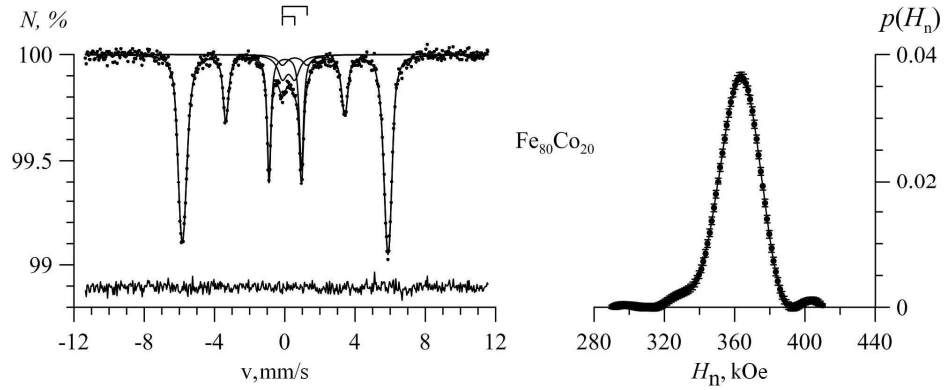

(b)

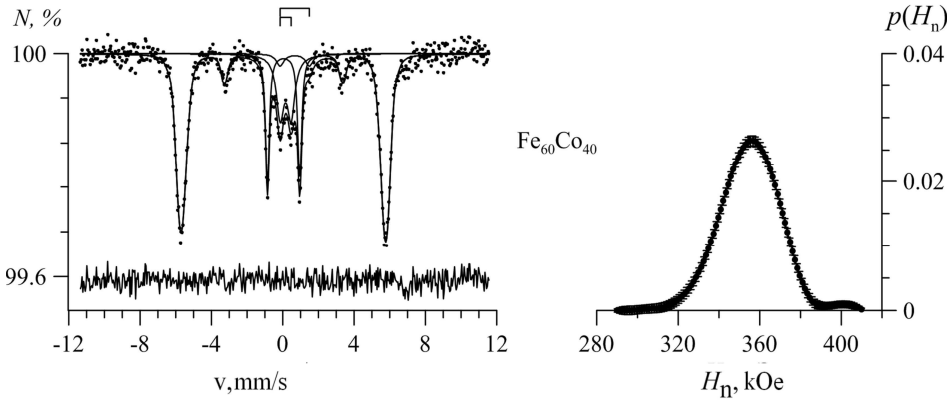

(c)

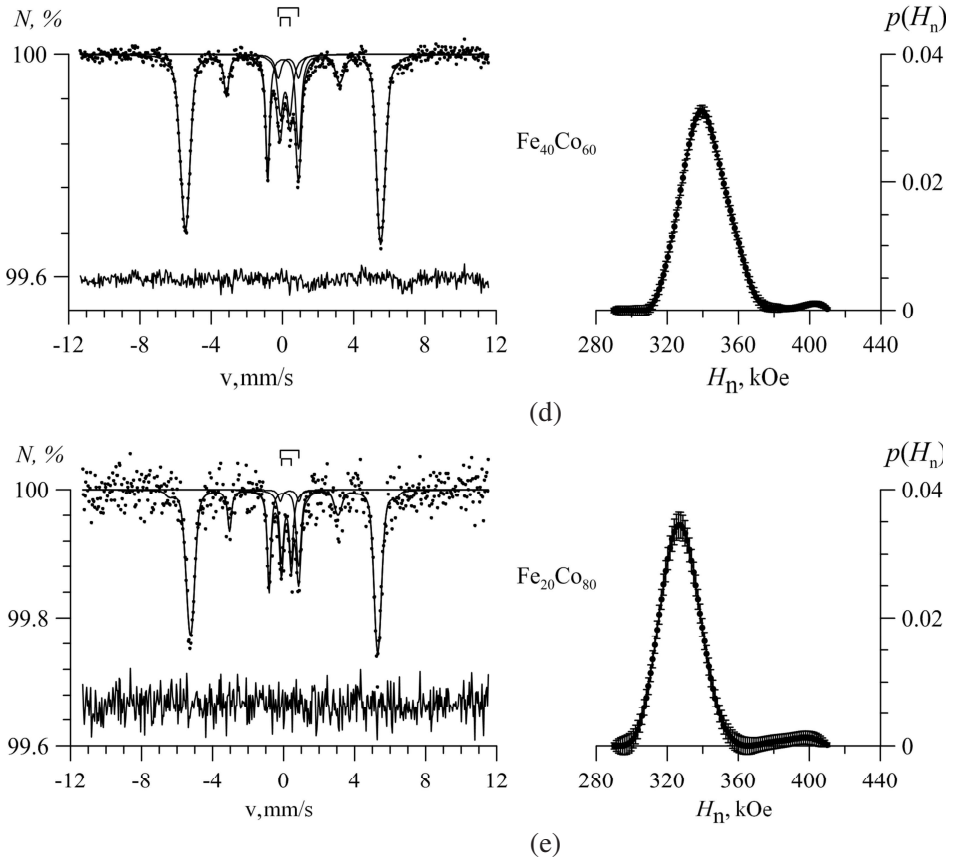

Figure 4. Results of the reconstruction of the $p(H_n)$ distributions of the hyperfine magnetic field H_n for Mossbauer spectra of ^{57}Fe nuclei in samples of $Fe_{100-x}Co_x$ nanotubes: (a) $Fe_{100}Co_0$; (b) $Fe_{82.46}Co_{17.54}$; (c) $Fe_{59.46}Co_{40.54}$; (d) $Fe_{40.29}Co_{59.71}$; (e) $Fe_{18.91}Co_{81.09}$.

$Fe_{100-x}Co_x$ nanotubes in a magnetic field.

Mossbauer studies were conducted to identify the local magnetic texture inside $Fe_{100-x}Co_x$ nanotubes. The samples of the nanotube arrays in PET for measurements were placed in such way that the nanotube axes were parallel to the direction of flight of γ-quantum. All measurements were provided at room temperature. The obtained Mossbauer spectra of ^{57}Fe nuclei in $Fe_{100-x}Co_x$ nanotubes represented Zeeman sextets with inhomogeneously broadened lines due to the existence of nonequivalent positions of iron atoms in nanotube structure. The method for reconstructing distributions of hyperfine parameters of Mossbauer spectra and model identification fitting using a priori information about the study object were used for processing of the Mossbauer spectra. Reconstructing distribution of hyperfine magnetic field $p(H_n)$ for main contribution to Mossbauer spectrum was made by modified Hesse-Rubartsch method, whose software implementation is described in reference [29].

In the general case, the spectra were a Zeeman sextet with broadened resonance lines and two quadrupole doublets (Figure 4). All spectra were processed by the method of reconstructing the distribution of hyperfine magnetic field and by the method of model decoding.

The Mossbauer spectrum (on the left) for $Fe_{100}Co_0$ nanotubes and the reduced distribution $p(H_n)$ of the hyperfine magnetic field H_n (on the right) are shown in Figure 4(a). It can be seen that the maximum of the reduced distribution of the hyperfine magnetic field is reached at $H_n \cong 330\,\mathrm{KOe}$. The mean values of the shift δ of Mossbauer line and the quadrupole displacement ε for the Zeeman sextet are close to zero ($\bar{\delta} = 0.004 \pm 0.003\,\mathrm{mm/s}$, $\bar{\varepsilon} = 0.001 \pm 0.003\,\mathrm{mm/s}$, and $H_n = 329.7 \pm 0.4\,\mathrm{KOe}$). Consequently, in accordance with well-known literature data for reference absorbers, the Zeeman sextet corresponds to α-Fe. The values of shifts of quadrupole doublets make it possible to identify them as partial spectra of Fe^{3+} cations in the paramagnetic high-spin state. In this connection, we can make

the assumption that Fe^{3+} cations belong to the paramagnetic iron salts used or obtained in samples synthesis.

For $Fe_{100-x}Co_x$ nanotubes, Mossbauer spectra and reconstructed hyperfine magnetic field distributions are shown in Figures 4(b)–(e). It can be seen that the hyperfine parameters differ from the values for $Fe_{100}Co_0$ samples of nanotubes. A similar pair of partial paramagnetic-type spectra corresponding to Fe^{3+} cations is observed for all samples of $Fe_{100-x}Co_x$ nanotubes.

From the concentration dependence of the average angle between the magnetic moment and the nanotube axis (Figure 5), it follows that for $Fe_{100}Co_0$ nanotubes a random distribution of the directions of the magnetic moments of Fe atoms is observed, and for $Fe_{100-x}Co_x$ nanotubes, a magnetic texture along the nanotube axis is observed. When the concentration of Co atoms increases, the average value of the angle between the direction of the magnetic moment of iron atoms and the axis of the nanotubes decreases from $\vartheta = 54.6°$ to $\vartheta = 24.5°$.

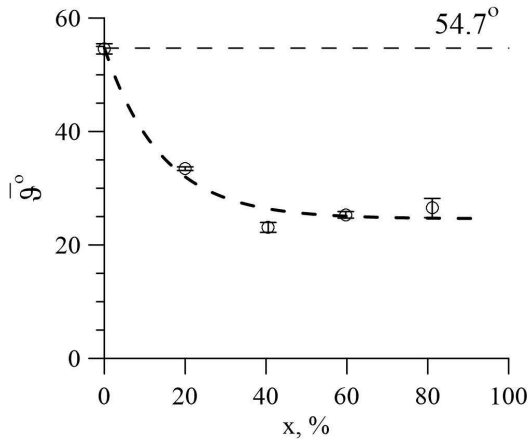

Figure 5. Graph of the concentration dependence of the average angle between the magnetic moment and the nanotube axis.

These results can be used for tailoring the magnetic properties of $Fe_{100-x}Co_x$ magnetic nanotubes electrodeposited in nanoporous templates. The observed effects can also be extended to another type of nanostructures or other materials, combining electrodeposition with advanced techniques as electron beam lithography.

4. CONCLUSION

Hollow nanostructures based on the $Fe_{100-x}Co_x$ alloy were synthesized in the pores of polymer templates based on PET using the electrochemical deposition method. The dependence of the change in structural and magnetic properties on the atomic content of the components in the nanotube structure is revealed. It is established that the synthesized nanostructures are hollow $Fe_{100-x}Co_x$ nanotubes with a body-centered cubic crystal structure (space group) with a unit cell parameter different from the reference value. The decrease in the unit cell parameter is due to the difference in the radii of the Fe (1.227 Å) and Co (1.191 Å) atoms. It is established that for $Fe_{100}Co_0$ nanotubes a random distribution of the directions of the magnetic moments of Fe atoms is observed, and for $Fe_{100-x}Co_x$ nanotubes, a magnetic texture along the nanotube axis is observed.

These results can be used for tailoring the magnetic properties of $Fe_{100-x}Co_x$ magnetic nanotubes electrodeposited in nanoporous templates. The observed effects can also be extended to another type of nanostructures or other materials, combining electrodeposition with advanced techniques as electron beam lithography.

REFERENCES

1. Ohgai, T., X. Hoffer, A. Fabian, L. Gravier, and J.-P. Ansermet, "Electrochemical synthesis and magnetoresistance properties of Ni, Co and Co/Cu nanowires in a nanoporous anodic oxide layer on metallic aluminium," *Journal of Materials Chemistry*, Vol. 13, No. 10, 2530, 2003.
2. Cristea, C., M. Tertis, and R. Galatus, "Magnetic nanoparticles for antibiotics detection," *Nanomaterials*, Vol. 7, No. 6, 119, 2017.
3. Wang, P., M. Du, M. Zhang, H. Zhu, S. Bao, M. Zou, and T. Yang, "Facile fabrication of AuNPs/PANI/HNTs nanostructures for high-performance electrochemical sensors towards hydrogen peroxide," *Chemical Engineering Journal*, Vol. 248, 307–314, 2014.
4. Li, C., X. Li, X. Duan, G. Li, and J. Wang, "Halloysite nanotube supported Ag nanoparticles heteroarchitectures as catalysts for polymerization of alkylsilanes to superhydrophobic silanol/siloxane composite microspheres," *Journal of Colloid and Interface Science*, Vol. 436, 70–76, 2014.
5. Denisova, E., L. Chekanova, R. Iskhakov, S. Komogortsev, I. Nemtsev, D. Velikanov, and S. Melnikova, "Magnetic anisotropy of co-nanostructures embedded in matrices with different pores size and morphology," *Solid State Phenomena. Trans. Tech. Publications*, Vol. 233, 583–586, 2015.
6. Graham, L. M., S. Cho, S. K. Kim, M. Nokeda, and S. B. Lee, "Role of boric acid in nickel nanotube electrodeposition: A surface-directed growth mechanism," *Chemical Communications*, Vol. 50, No. 5, 527–529, 2014.
7. Liao, S. H., K. L. Chen, C. M. Wang, J. J. Chieh, H. E. Horng, L. M. Wang, C. H. Wu, and H. C. Yang, "Using bio-functionalized magnetic nanoparticles and dynamic nuclear magnetic resonance to characterize the time-dependent spin-spin relaxation time for sensitive bio-detection," *Sensors*, Vol. 14, No. 11, 21409–21417, 2014.
8. Yen, S. K., P. Padmanabhan, and S. T. Selvan, "Multifunctional iron oxide nanoparticles for diagnostics, therapy and macromolecule delivery," *Theranostics*, Vol. 3, No. 12, 986, 2013.
9. Dragos, O., H. Chiriaca, N. Lupua, M. Grigorasa, and I. Tabakovic, "Anomalous codeposition of fcc NiFe nanowires with 5–55% Fe and their morphology, crystal structure and magnetic properties," *Journal of The Electrochemical Society*, Vol. 163, No. 3, D83–D94, 2016.
10. Frolov, K. V., D. L. ZagorskiiI, S. Lyubutin, M. A. Chuev, I. V. Perunov, S. A. Bedin, A. A. Lomov, V. V. Artemov, and S. N. Sulyanov, "Magnetic and structural properties of Fe-Co nanowires fabricated by matrix synthesis in the pores of track membranes," *JETP Letters*, Vol. 105, No. 5, 319–326, 2017.
11. Evans, P. R. and Y. G. Schwarzacher, "Current perpendicular to plane giant magnetoresistance of multilayered nanowires electrodeposited in anodic aluminum oxide membranes," *Applied Physics Letters*, Vol. 76, No. 4, 481–483, 2000.
12. Qin, J., J. Nogues, M. Mikhaylova, A. Roig, J. S. Munoz, and M. Muhammed, "Differences in the magnetic properties of Co, Fe, and Ni 250–300 nm wide nanowires electrodeposited in amorphous anodized alumina templates," *Chemistry of Materials*, Vol. 17, No. 7, 1829–1834, 2005.
13. Guo, P., X. Chen, W. Guan, H. Cheng, and H. Jiang, "Effect of tensile stress on the variation of magnetic field of low-alloy steel," *Journal of Magnetism and Magnetic Materials*, Vol. 323, No. 20, 2474–2477, 2011.
14. Vivas, L. G., Y. P. Ivanov, D. G. Trabada, M. P. Proenca, O. Chubykalo-Fesenko, and M. Vazquez, "Magnetic properties of Co nanopillar arrays prepared from alumina templates," *Nanotechnology*, Vol. 24, No. 10, 105703, 2013.
15. Peppas, N. A., J. Z. Hilt, A. Khademhosseini, and R. Langer, "Hydrogels in biology and medicine: From molecular principles to bionanotechnology," *Advanced materials*, Vol. 18, No. 11, 1345–1360, 2006.
16. Ripamonti, C. I., D. Santini, E. Maranzano, M. Berti, and F. Roila, "Management of cancer pain: ESMO clinical practice guidelines," *Annals of Oncology*, Vol. 23, No. 7, vii139–vii154, 2012.
17. Zhang, L., T. Petit, K. E. Peyer, and B. J. Nelson, "Targeted cargo delivery using a rotating nickel nanowire," *Nanomedicine: Nanotechnology, Biology and Medicine*, Vol. 8, No. 7, 1074–1080, 2012.

18. Zdorovets, M., I. Ivanov, M. Koloberdin, S. Kozin, V. Alexandrenko, E. Sambaev, and A. Kurakhmedov, "Accelerator complex based on DC-60 cyclotron," *Proc. 24th Russian Particle Accelerator Conf.*, 287–289, 2014.
19. Kaniukov, E. Y., E. E. Shumskaya, D. V. Yakimchuk, A. L. Kozlovskiy, M. A. Ibragimova, and M. V. Zdorovets, "Evolution of the polyethylene terephthalate track membranes parameters at the etching process," *J. Contemp. Phys.*, Vol. 52, 155–160, 2017.
20. Matsnev, M. E. and V. S. Rusakov, "SpectrRelax: An application for Mossbauer spectra modeling and fitting," *AIP Conference Proceedings, AIP*, Vol. 1489, No. 1, 178–185, 2012.
21. Shao, P., G. Ji, and P. Chen, "Gold nanotube membranes: Preparation, characterization and application for enantioseparation," *Journal of Membrane Science*, Vol. 255, No. 1, 1–11, 2005.
22. Yu, T., Z. X. Shen, Y. Shi, and J. Ding, "Cation migration and magnetic ordering in spinel $CoFe_2O_4$ powder: Micro-Raman scattering study," *Journal of Physics: Condensed Matter*, Vol. 14, No. 37, L613, 2002.
23. Chen, Z., Q. Zhan, D. Xue, F. Li, X. Zhou, H. Kunkel, and G. Williams, "Mossbauer study of Fe-Co nanowires," *Journal of Physics: Condensed Matter*, Vol. 14, No. 3, 613, 2002.
24. Hunter, D., W. Osborn, K. Wang, N. Kazantseva, J. Hattrick-Simpers, R. Suchoski, R. Takahashi, M. L. Young, A. Mehta, L. A. Bendersky, S. E. Lofland, M. Wuttig, and I. Takeuchi "Giant magnetostriction in annealed $Co_{1-x}Fe_x$ thin-films," *Nature Communications*, Vol. 2, 518, 2011.
25. Pearson, W. B., *A Handbook of Lattice Spacings and Structures of Metals and Alloys*, Pergamon, New York and Oxford, 1966.
26. Harris, G. B., "Quantitative measurement of preferred orientation in rolled uranium bars," *Dublin Philosophical Magazine and Journal of Science*, Vol. 43, No. 336, 113, 1952.
27. Ahmad, N., A. Saeeda, S. Khana, F. Hassana, W. J. Lib, S. A. Shahc, A. Majidd, and X. F. Hanb, "Investigation of easy axis transition and magnetodynamics in $Ni_{76}Fe_{24}$ nanowires and $Ni_{77}Fe_{23}$ nanotubes synthesized by DC electrodeposition," *Journal of Alloys and Compounds*, Vol. 725, 123e128, 2017.
28. Irfan, M., U. Khan, W. Li, N. Adeela, K. Javed, and X. F. Hana, "Magnetic investigations of post-annealed metallic Fe nanowires via electrodeposition method," *Materials Letters*, Vol. 180, 235–238, 2016.
29. Piraux, L., J. M. George, J. F. Despres, C. Leroy, E. Ferain, and R. Legras, "Giant magnetoresistance in magnetic multilayered nanowires," *Applied Physics Letters*, Vol. 65, No. 19, 2484–2486, 1994.